Mesoporous Nickel−Yttria−Zirconia Fuel Cell Materials

Marc Mamak, Neil Coombs, and Geoffrey A. Ozin*

Materials Chemistry Research Group, Chemistry Department, University of Toronto, 80 St. George Street, Toronto, Ontario M5S 3H6, Canada

Received January 10, 2001

A novel synthesis method for mesoporous nickel−yttria−zirconia (meso-Ni−YZ) has been developed using a surfactant-templated co-assembly strategy, involving yttrium(III)−zirconium(IV) glycometalate and nickel(II) precursors. Nickel loading has been investigated over the range 0−45 Ni at. % and found to control the average pore size of the oxidized meso-NiO_{1+x}−YZ and reduced meso-Ni−YZ products. Under the synthesis conditions utilized, the cationic surfactant glycometalate co-assembly is proposed to involve nickel in the form of $Ni_4(OH)_4^{4+}$, which subsequently transforms to a co-assembly containing nanoscale $Ni(OH)_2$. Upon thermal posttreatment in air, the nickel hydroxide species is converted to the nanocrystalline p-type nickel oxide, $NiO_{1+x,}$ located in the pores of meso-NiO_{1+x}−YZ. The channel walls of meso-NiO_{1+x}−YZ are composed of nanocrystalline yttria−zirconia, and the gas adsorption isotherm appears as type I. Thermal reduction of the NiO_{1+x} component of the mesostructure in hydrogen creates nickel nanocrystals. A concomitant dramatic increase in average pore diameter is observed with concurrent evolution of an adsorption isotherm of type IV. This behavior is attributed to a structural transformation of meso-NiO_{1+x}−YZ to meso-Ni−YZ involving a reduction in NiO_{1+x} nanocrystal size on conversion to Ni with accompanying migration and aggregation of Ni nanocrystals. The outcome of these combined effects widens the pores within meso-Ni−YZ relative to meso-NiO_{1+x}−YZ. Preliminary ac impedance spectroscopy of meso-Ni−YZ at a loading of less than 40 at. % Ni depicts an electrical response dominated by oxygen ion conductive nanocrystalline YZ channel walls of the meso-Ni−YZ mesostructure. By contrast, higher nickel loaded meso-Ni−YZ samples give a metallic response most likely due to a better connectivity of Ni nanocrystals within the mesostructure.

Introduction

Beginning with the discovery of MCM-41 mesoporous silica by Mobil Corp. in 1992, surfactant assemblies as micelles and liquid crystals have been used to template a variety of periodic mesoporous materials.[1] The composition of these materials include silica, organosilica, transition metal loaded silica, transition metal oxo-phosphates, and transition metal oxo-sulfates.[2] Generally, transition metal oxides prepared by these reported methods without structure stabilizing anions such as phosphate or sulfate groups have proven to be thermally unstable and collapse upon calcination with the possible exception of niobium and tantalum oxides prepared from the ligand assisted templating approach which reportedly collapse around 400 °C.[3] An analogous templating method employs amphiphilic poly(alkylene oxide) block copolymers as structure-directing agents and inorganic chloride salts as oxide precursor.[4] The mesostructured materials formed during this kind of preparation are thermally stable due to relatively thick and nanocrystalline walls, which prevent structural collapse. Recently, we have reported the synthesis and characterization of a new class of binary and ternary mesoporous materials denoted meso-M−YZ, where M = Pt or NiO_{1+x} and YZ stands for a solid-solution of yttria−zirconia.[5] These materials were prepared by a co-assembly synthetic strategy using glycometalate and metal precursors in the presence of a cationic surfactant template and under aqueous conditions. Meso-M−YZ materials were discovered to exhibit unusually high thermal stability for a mesoporous transition metal oxide prepared from a cationic surfactant, which was attributed to concurrent crystallization and thickening of YZ walls as the surfactant is lost to thermal oxidation in air to yield a nanocrystalline mesostructured material. Materials of this genre were found to exhibit type I behavior from nitrogen adsorption/desorption isotherms, indicating the presence of microporosity rather than the expected type IV mesoporous behavior. The average pore sizes for these materials were found to be 18−22 Å straddling the micro- and mesoscopic regime.

(1) (a) Kresge, C. T.; Leonowicz, M. E.; Roth, W. J.; Vartuli, J. C.; Beck, J. S. *Nature* **1992**, 359, 710. (b) Beck, J. S.; Vartuli, J. C.; Roth, W. J.; Leonowicz, M. E.; Kresge, C. T.; Schmitt, K. D.; Chu, C. T.-W.; Olson, D. H.; Sheppard, E. W.; McCullen, S. B.; Higgins, J. B.; Schlenker, J. L. *J. Am. Chem. Soc.* **1992**, *114*, 10834.

(2) See for example: (a) Sayari, A.; Liu, P. *Micropor. Mater.* **1997**, *12*, 149. (b) Ying, J. Y.; Mehnert, C. P.; Wong, M. S. *Angew. Chem., Int. Ed.* **1999**, *38*, 56.

(3) (a) Antonelli, D. M.; Ying, J. Y. *Angew. Chem., Int. Ed. Engl.* **1996**, *35*, 426. (b) Antonelli, D. M. *Chem. Mater.* **1996**, *8*, 874. (c) Antonelli, D. M.; Nakahira, A.; Ying, J. Y. *Inorg. Chem.* **1996**, *35*, 3126.

(4) (a) Yang, P.; Zhao, D.; Margolese, D. I.; Chmelka, B. F.; Stucky, G. D. *Nature* **1998**, *396*, 152. (b) Yang, P.; Zhao, D.; Margolese, D. I.; Chmelka, B. F.; Stucky, G. D. *Chem. Mater.* **1999**, *11*, 2813.

(5) (a) Mamak, M.; Coombs. N. Ozin, G. *Adv. Mater.* **2000**, 12, 198. (b) Mamak, M.; Coombs, N.; Ozin, G. *J. Am. Chem. Soc.* **2000**, 122, 8932. (c) Mamak, M.; Coombs, N.; Ozin, G. *Adv. Funct. Mater.* **2001**, *11*, 59.

10.1021/cm001259j CCC: $20.00
Published on Web 09/05/2001

Although there is much interest in the possible use of mesoporous metal oxides in catalytic, electrocatalytic, electrochromic, charge transport, optical, and host−guest inclusion applications, in this particular study we are interested in meso-Ni−YZ as a potential low-temperature, solid oxide fuel cell (SOFC) electrode material. To amplify, all SOFC anodes must combine an electronic conductor with an oxygen ion conductor in order to oxidize the gaseous fuel and allow the electrons to flow around the open circuit.[6] Currently the anode material of choice is a metal−ceramic composite, denoted Ni−YZ cermet, where the Ni provides electronic conduction while the YZ portion provides oxygen ion conduction. The electrocatalytic reaction occurs at the triple phase boundary (TPB), an interface within this composite at the junction between the electronic conductor, ionic conductor, and gaseous reactants.[7] The length of the TPB is mainly responsible for polarization processes occurring at the electrodes. Usually the Ni−YZ cermet is an engineered composite where powders of NiO and YZ are sintered together before NiO is reduced to Ni. Typical dimensions of the resulting grains are about 1−5 μm, and the porosity resulting from the volume reduction of NiO to Ni is at best 30 m^2/g. The porosity of the cermet serves two functions. The first is to allow for easy diffusion of gaseous reactants into the cermet microstructure, and the second is to lengthen the TPB region by increasing the number of interfaces between Ni, YZ, and the gaseous reactants. Both of these functions improve the efficiency of the SOFC by increasing mass transport (i.e., gaseous diffusion, adsorption processes, and surface diffusion) and creating a longer boundary region over which charge-transfer processes can occur. It has been found that reduction in the dimension of the metal grains relative to the YZ ones gives a larger TPB length.

Herein we report the synthesis and characterization of mesoporous nickel−yttria−zirconia, denoted meso-Ni−YZ, containing nickel in the reduced metallic form for the first time and an investigation of the structural, stability, and electrical properties at nickel loading as high as 45 at. %. This new class of a ternary mesoporous material displays the highest surface area for any known composite of nickel metal−yttria−zirconia. This material may be of interest for use as an anode in low-temperature SOFCs. The process for forming meso-Ni−YZ with mesoscale pores and channel walls comprised of nanocrystalline nickel and yttria−zirconia is novel. It is to be contrasted with earlier work from our laboratory on synthesis of meso-Pt−YZ and meso-NiO_{1+x}−YZ in which the pore sizes straddled the microscopic and mesoscopic regimes and the channel walls were based on nanocrystalline platinum and p-doped nickel oxide, respectively, in combination with nanocrystalline yttria−zirconia.

Experimental Section

(a) Preparation of Meso-Ni−YZ. A 5 g amount of zirconium ethoxide (99+%, Strem) and 1.66 g NaOH was added to 50 mL of ethylene glycol (99.9%, Aldrich). This mixture was refluxed overnight under flowing nitrogen to form a clear solution, after which, excess ethylene glycol was distilled off, creating a thick, clear gel denoted as zirconium glycolate.[8] Separately, 1.2 g of anhydrous yttrium acetate (99.9%, Alfa) was added to 30 mL of ethylene glycol. This mixture denoted yttrium glycolate became clear within 30 min while being stirred under nitrogen. The zirconium and yttrium species were then added together in a dropwise fashion, forming a much thicker white, gelatinous species denoted YZ glycolate. Typically, one-quarter to one-fifth of this gel was added to a polypropylene bottle containing 30 mL of H_2O, 1 g of cetyltrimethylammonium bromide (CTAB; Aldrich), and 0.4 g of NaOH. Either nickel acetate, nickel nitrate, or nickel chloride was predissolved in warm ethylene glycol. This green solution was then added to a polypropylene bottle. After the mixtures were stirred initially for 20 min, each bottle was heated at 80 °C for 1−5 days. The contents of the bottles were recovered by vacuum filtration and were washed with distilled water. The as-synthesized powder cake was green in color and turned black after calcination at 450 °C in air. A reduction of the NiO was carried out by placing the meso-NiO−YZ sample in a tube furnace under pure flowing hydrogen gas using a 3 h heating ramp to 400 °C and holding it there for 10 h.

(b) Characterization of Meso-Ni−YZ. Powder X-ray diffraction (PXRD) data were obtained on a Siemens D5000 diffractometer using Ni filtered Cu Kα radiation ($\lambda = 1.541\ 78$ Å) with a Kevex 2005−22 solid-state detector. Variable temperature (VT) PXRD data were obtained by using the variable temperature stage attachment. Transmission electron microscopy (TEM) images were obtained on a Phillips 430 microscope operating at 100 kV. Samples were embedded in an epoxy-based resin, cured at 60 °C for 24 h and sectioned using an ultra-microtome and a diamond knife. High resolution field emission TEM (HR-FE-TEM) was done on a JEOL 210F field emission microscope operating at an accelerating voltage of 200 kV. Nitrogen adsorption and desorption isotherms were performed at 77 K. All samples were outgassed at 200 °C. Average pore diameters were determined using the BJH method. Complex impedance measurements were carried out using a Solartron frequency response analyzer Model 1260. Meso-Ni−YZ samples were pressed into a pellet and electrical contacts were affixed using Pt ink (Englehard # 6082) and Pt mesh. All samples were loaded in a measurement rig within a quartz chamber designed for flowing through various gases. This rig was placed in a DC top-loading high-temperature oven. All samples were analyzed from 0.1 to 10^7 Hz using an ac amplitude of 0.5 mV starting from 300 °C under an atmosphere of flowing 5% H_2/N_2 gas mixture (Matheson). Automated acquisition was facilitated by ZPLOT Version 2.1a (Scribner Associates) software, and subsequent analysis was performed using ZVIEW Version 1.5 (Scribner Associates).

Results and Discussion

A series of meso-NiO_{1+x}−YZ samples with p-type nickel oxide content ranging from 16 to 45 mol % were synthesized as previously reported. In the as-synthesized form, meso-NiO_{1+x}−YZ samples were green in color and transparent and had a brittle plastic to glasslike textural appearance. All samples in the as-synthesized form gave an invariant first PXRD *d* spacing of about 40 Å. Upon calcination, however, this *d* spacing grows as a function of NiO loading, as seen in Figure 1. The calcined samples appear as a homogeneous black powder, which is a color characteristic for the p-type oxide, NiO_{1+x}.[9] The first *d* spacing ranges from 93 Å for the highest loaded sample to 51 Å for a

(6) (a) Minh, N. Q. *J. Am. Ceram. Soc.* **1993**, 76, 563. (b) Takahashi, T.; Minh, N. Q. *Science and Technology of Ceramic Fuel Cells*; Elsevier: New York, 1995.

(7) (a) Verweij, H. *Adv. Mater.* **1998**, *10*, 1483. (b) Ziehfreund, A.; Simon, U.; Maier, W. F. *Adv. Mater.* **1996**, *8*, 424. (c) van Berkel, F. P. F.; van Heuveln, F. H.; Huijsmans, J. P. P. *Solid State Ionics* **1994**, *72*, 240. (d) Steele, B. C. H. *Solid State Ionics* **1997**, *94*, 239.

(8) Khushalani, D.; Ozin, G. A.; Kuperman, A. J. *J. Mater. Chem.* **1999**, *9*, 1491.

(9) West, A. R. *Solid State Chemistry and Its Applications*; John Wiley & Sons Ltd.: New York, 1984.

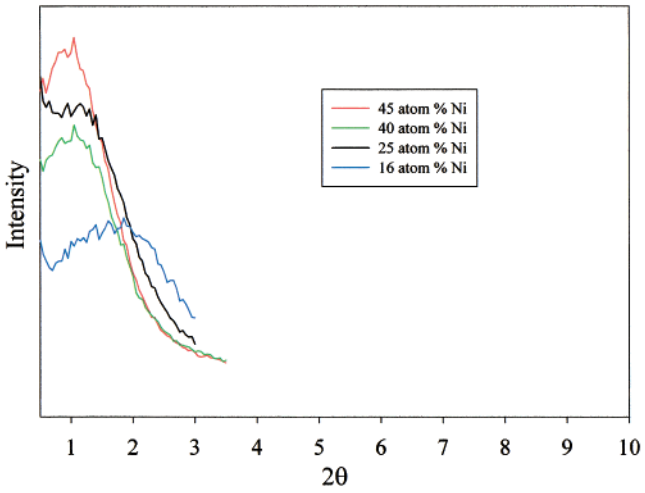

Figure 1. Low-angle PXRD pattern of meso-Ni−YZ containing 16−45 Ni at. %.

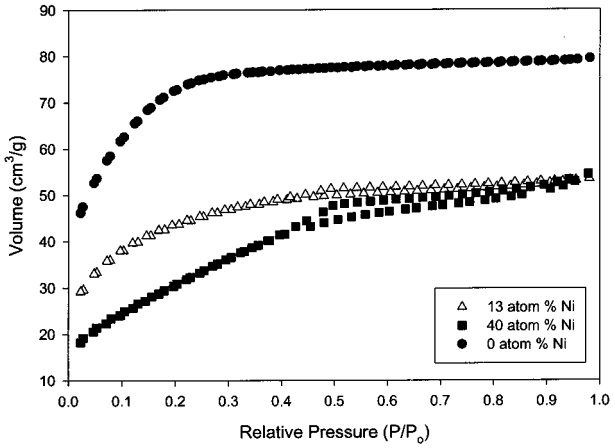

Figure 2. Nitrogen gas adsorption isotherms (77 K) of meso-NiO_{1+x}–YZ samples containing 0−40 atom % Ni.

13 mol % loaded sample. At higher PXRD 2θ extremely broad peaks are observed, which can be assigned to a YZ phase and a NiO phase. The YZ pattern matches best with the cubic phase (JCPDS No. 30-1468), which is reasonable for a solid solution composition of 9 mol % Y_2O_3. The 111 and 200 reflections overlap, which makes particle size determination difficult. An accurate determination of particle size is also not possible for the NiO phase due to the 111 reflection of the NiO phase (JCPDS No. 02-1216) overlapping with the 200 YZ reflection combined with an extremely broad 200 NiO reflection. Our best estimate of NiO and YZ crystallite size based on PXRD line widths in conjunction with a TEM analysis is of the order of 20−40 Å.

An attempt at better elucidating the position of NiO_{1+x} within the YZ phase as well as gaining a sense of structural order begins with an examination of information derived from gas adsorption isotherms. Figure 2 shows representative isotherms for meso-YZ and meso-NiO_{1+x}−YZ. Except for the NiO_{1+x} loading, each version of the mesostructure was synthesized and calcined in an identical manner. At first glance, the isotherm for meso-YZ most closely resembles type I behavior indicative of a microporous sample; however, the isotherm does not level off below a relative pressure of 0.1.[10] It is known that mesoporous materials which have a pore size close to the micropore range (<20 Å) can result in type I behavior. Our material continues to adsorb up to a minimum relative pressure of 0.2 and, therefore, most probably contains of a fair amount of mesopores.[10b] One explanation for the isotherm observed for meso-YZ may be that this material consists of pores with a size distribution near the micro-/meso-demarcation where both type I and type IV responses are observed to some extent. The possibility of an ordered system of mesopores with a secondary system of pores such as micropores formed between at the grain boundary of YZ nanocrystallites, for example, cannot be dismissed at this stage. Upon the addition of NiO_{1+x} one observes a change in the general shape of the isotherm along with a decrease in the total adsorbed volume. Hysteresis between adsorption and desorption branches as well as increased adsorption above 0.1 partial pressure becomes increasingly evident from the 13 to the 40 Ni at. % isotherm, indicating more of a tendency toward type IV behavior as the NiO_{1+x} content increases. Table 1 emphasizes this trend by showing results for a series of samples of varying NiO_{1+x} content from 0 to 40 mol %, where the average pore diameter starts at 18 Å and grows to 30 Å.[11] At this point of the discussion, it is important to make the point that the NiO_{1+x} content has a direct influence upon the average pore size and the type of isotherm. This implies that nanocrystalline NiO_{1+x} is most likely associated with the pores and influences the co-assembly/calcination process of the YZ phase to yield larger pores.

Table 1

Ni at. %	BET SA (m^2/g)	av pore size (Å)
0	264	18.6
13	156	21.2
30	136	23.5
33	134	26.2
40	112	30.0

A slightly darker black powder was formed from the reduction of meso-NiO_{1+x}−YZ to yield a material denoted as meso-Ni−YZ. Figure 3 compares the PXRD pattern of this material before and after reduction. The process of reduction has little effect on the crystallinity of the YZ phase by comparing the broad peak at about 30° 2θ, which is composed of overlapping 111 and 200 peaks. After reduction, broad NiO_{1+x} reflections disappear and only the (111) and (200) reflections for metallic nickel are observed. Similarly, the reduced species meso-Ni−YZ maintains a low-angle reflection at about the same *d* spacing as that observed before reduction in meso-NiO_{1+x}−YZ, Figure 4. This reflection can be at-

(10) (a) Gregg, S. J.; Sing, K. S. W. *Adsorption, Surface Area, and Porosity;* Academic Press Ltd.: London, 1982. (b) Kruk, M.; Jaroniec, M. *Chem. Mater.*, in press.

(11) Note to reader: BET and BJH methods of determining surface area and average pore size are common methods for analyzing the surface properties of mesoporous materials and are not to be taken as accurate for the analysis of microporous materials. However, as explained in the text, the materials summarized in Table 1 show an adsorption response of a material containing a fair amount of mesopores. This is increasingly evident for samples containing NiO_{1+x} loadings above 13 mol % where isotherms more similar to type IV are observed. With regard to samples containing less than 13 mol % NiO_{1+x}, while it is difficult to account for the presence of micropores or the effect of mesopores close to the micropore regime in BET or BJH analysis, the findings presented in Table 1 are meant to provide the reader with data for comparison with samples of other NiO_{1+x} loadings and to show a trend. It is up to the reader to choose whether to take these at face value. See ref 10b for further discussion regarding the adsorption of mesoporous materials close to the microregime.

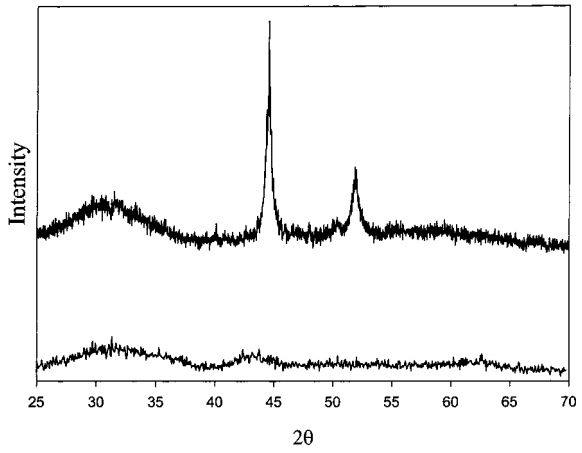

Figure 3. High-angle PXRD pattern comparing meso-NiO_{1+x}–YZ (bottom) and meso-Ni−YZ (top).

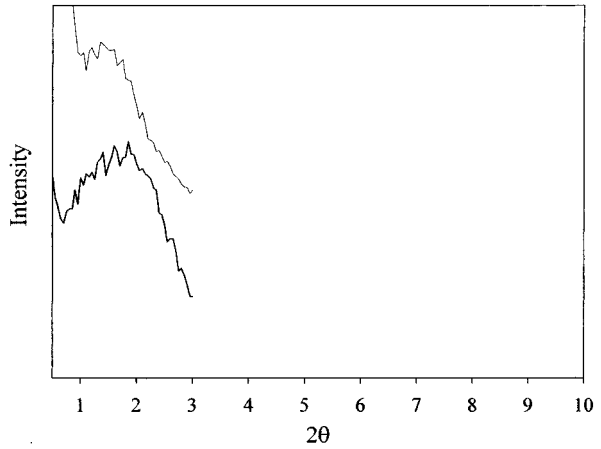

Figure 4. Low-angle PXRD pattern comparing meso-NiO_{1+x}–YZ (bottom) and meso-Ni−YZ (top).

tributed to the average pore wall-to-pore wall repeat distance arising from long-range order in a periodic meso-Ni−YZ mesostructure. This suggests structural order at the mesoscopic length scale remains essentially undisturbed following reduction of meso-NiO_{1+x}−YZ to meso-Ni−YZ.

The TEM micrographs depicted in Figure 5 compare meso-NiO_{1+x}−YZ with the reduced version meso-Ni−YZ. Before reduction, ordering at the mesoscale is evident and can be best described as a worm-hole structure with a random network of pores.[12] Closer inspection shows 30−60 Å clusters of darker contrast distributed throughout the worm-hole structure, which we originally believed to be associated with a dense NiO_{1+x} phase as these areas of darker contrast are absent in YZ-phase pure material. Surprisingly, a dramatic improvement in mesoscale ordering is observed in the reduced version meso-Ni−YZ. The diffuse dark region superpositioned over the YZ mesostructure is metallic nickel as confirmed by energy-dispersive X-ray spectroscopy (EDX) spot analysis. It is evident from the micrograph that there has been considerable diffusion and aggregation of Ni during the reduction process. A particle size analysis from the Scherrer equation correlates well with the results of TEM analysis giving Ni cluster sizes ranging from 130 to 300 Å for the highest loaded sample. These particle sizes are four to ten times the estimated initial size of NiO_{1+x}, confirming diffusion and aggregation has taken place during hydrogen reduction. Most interesting is the fact that the pore structure of the reduced version is distinctly more visible.

EDX by SEM of meso-NiO_{1+x}−YZ shows NiO_{1+x} to be well-dispersed within the YZ phase. While there are regions that appear to have a slightly higher concentration of the NiO_{1+x}, phase, strict NiO_{1+x} and YZ phase segregation can be ruled out at this length scale. To further probe the homogeneity of the material, we used HR-FE-TEM EDX spot analysis and elemental mapping techniques on meso- NiO_{1+x}−YZ thin sections surveying the elemental landscape of the material. Specifically, we were concerned with the elemental composition of the areas of darker contrast versus the overall composition. Spot analysis of an area of darker contrast and a general region of about 100 times this area shows the Ni content to be somewhat higher in the dark contrast region; however Ni, Y, and Zr species are present to a considerable extent in both regions. Elemental mapping over different sample areas and magnifications gave no conclusive evidence for the presence of compositional gradients within the sample. Upon increased magnification, this material was found to be composed of a wormlike porous network of nanocrystallites, each on the order of 20−40 Å, most of which gave rise to well-resolved TEM lattice images. Extensive surveys of our samples have lead us to conclude that our material is composed of a porous nanocrystalline network devoid of large occluded dense phases which could be caused by the phase separation of either NiO_{1+x} or YZ species. Several EDX spot analyses were performed while the beam was trained on sample areas of about 30 Å in diameter. In no instance does one ever observe regions of pure YZ or NiO_{1+x}; however, there is a fairly constant ratio of Ni to Zr/Y at each location. To this end, we cannot conclusively attribute the regions of darker contrast observed in our material to a difference of atomic scattering factor arising from phase separation phenomena. This change of contrast may arise from diffraction contrast effects produced by the specific orientation of nanocrystallites resulting from the manner in which our sample fractured when microtomed into a thin section. In any event, our results indicate a very high dispersion of NiO_{1+x} at the nanometer length scale, leading to a homogeneous composite material denoted meso-NiO−YZ.

Nitrogen adsorption/desorption isotherms for a series of meso-Ni−YZ samples ranging from 16 to 45 at. % Ni are shown in Figure 6. A notable trend toward typical type IV behavior and increasing average pore size is observed upon increasing the loading of nickel. The 16 at. % sample has the widest pore size distribution with an average diameter centered at 25 Å. The associated isotherm appears to be a combination of type I and type IV, most likely the result of a wide distribution of pore sizes straddling microscale and mesoscale regimes. With each increasing Ni loading, type IV isotherm behavior is seen to dominate. Figure 7 shows a linear trend that correlates the Ni content and average pore size. Not only does average pore size increase but the pore size

(12) (a) Tanev, P. T.; Pinnavaia, T. J. *Science* **1995**, 267, 865. (b) Zhang, W.; Pauly, T. R. Pinnavaia, T. J. *Chem. Mater.* **1997**, *9*, 2491.

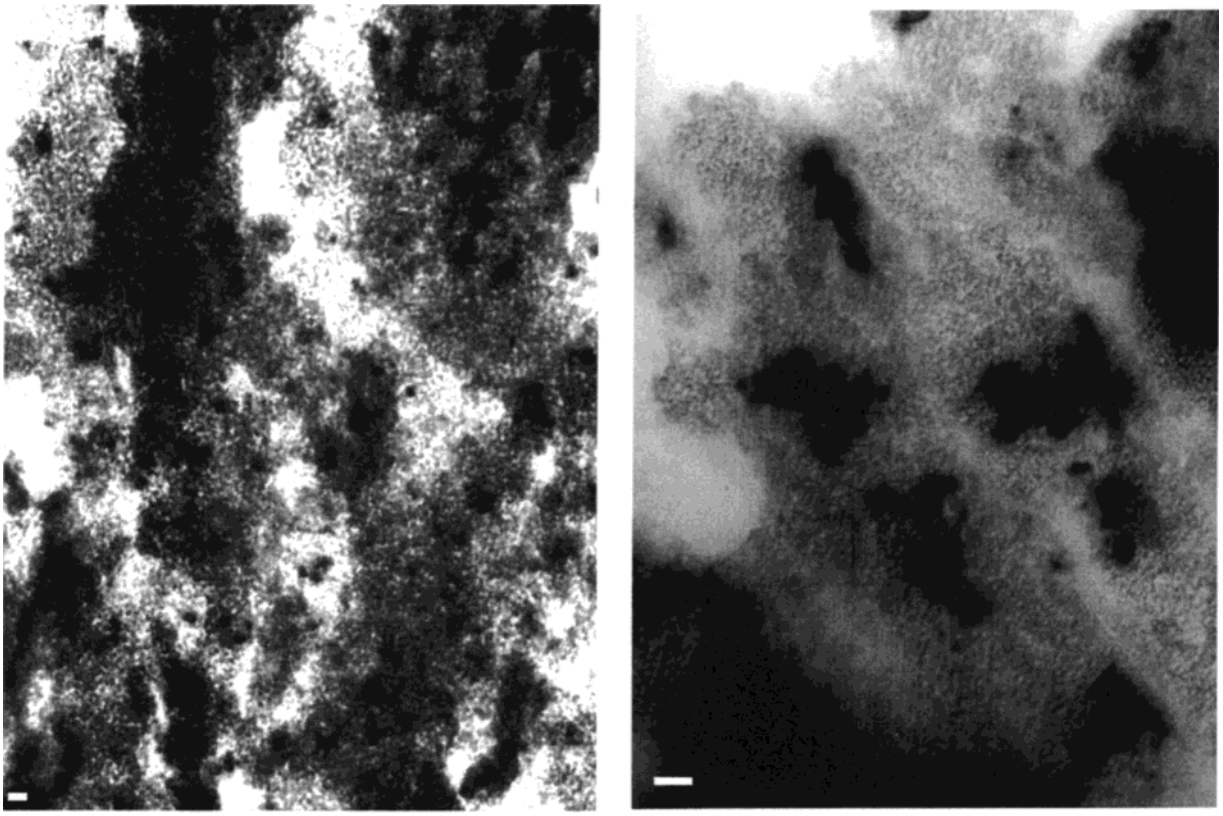

Figure 5. TEM images of microtomed thin sections of (left) meso-NiO_{1+x}–YZ (magnification bar = 11 nm) and (right) meso-Ni–YZ (magnification bar = 174 nm).

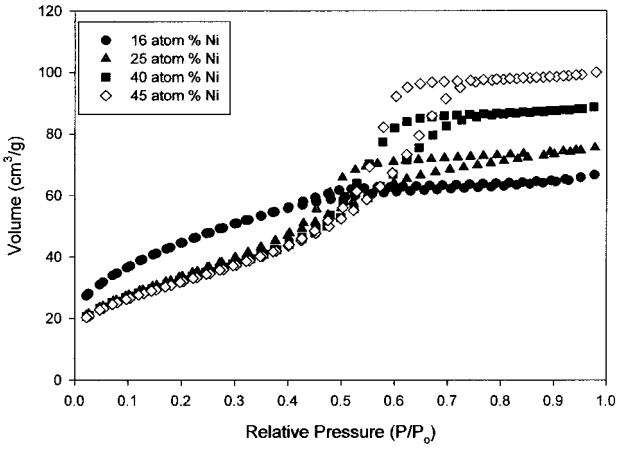

Figure 6. Nitrogen gas adsorption isotherms (77 K) of meso-Ni–YZ containing 16–45 Ni at. %.

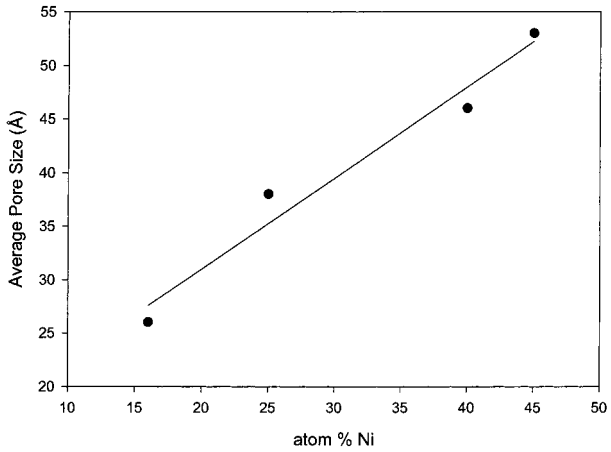

Figure 7. Plot of average pore size vs degree of Ni loading for meso-Ni–YZ.

distribution becomes remarkably smaller for each successive Ni loading and is in fact quite narrow at the highest loading. Table 2 summarizes some physical properties for the series of meso-Ni–YZ samples. BET surface area decreases initially from the 16 to the 25 at. % sample but remains fairly constant upon increasing the loading to 45 at. %. Both the average pore size and low-angle *d* spacing increase as a function of nickel content. The estimated wall thickness remains constant for the 25, 40, and 45 at. % Ni samples, which is an important point that will be further explored.

The incorporation of nickel, either as NiO_{1+x} or metallic nickel into meso-YZ, is seen to have an interesting effect on the pore structure. The key ideas are illustrated in Scheme 1. We attribute this effect to electrostatic interactions between the cationic surfactant, anionic YZ glycolate, and an aqueous cationic nickel intermediate phase involved in the original co-assembly process. Under basic aqueous conditions, Ni^{2+} is expected to be present in solution as $Ni_4(OH)_4^{+4}$.[13] Following the order of addition of precursors, the anionic YZ glycolate first interacts electrostatically with the

Table 2

Ni at. %	BET SA (m^2/g)	av pore size (Å)	*d* spacing (Å)	wall thickness (Å)
16	162	26	51	34
25	123	38	79	53
40	119	46	87	54
45	116	53	93	54

(13) Soler-Illia, G. J. de A.; Jobbagy, M.; Regazzoni, A. E.; Blesa, M. A. *Chem. Mater.* **1999**, *11*, 3140.

Scheme 1[a]

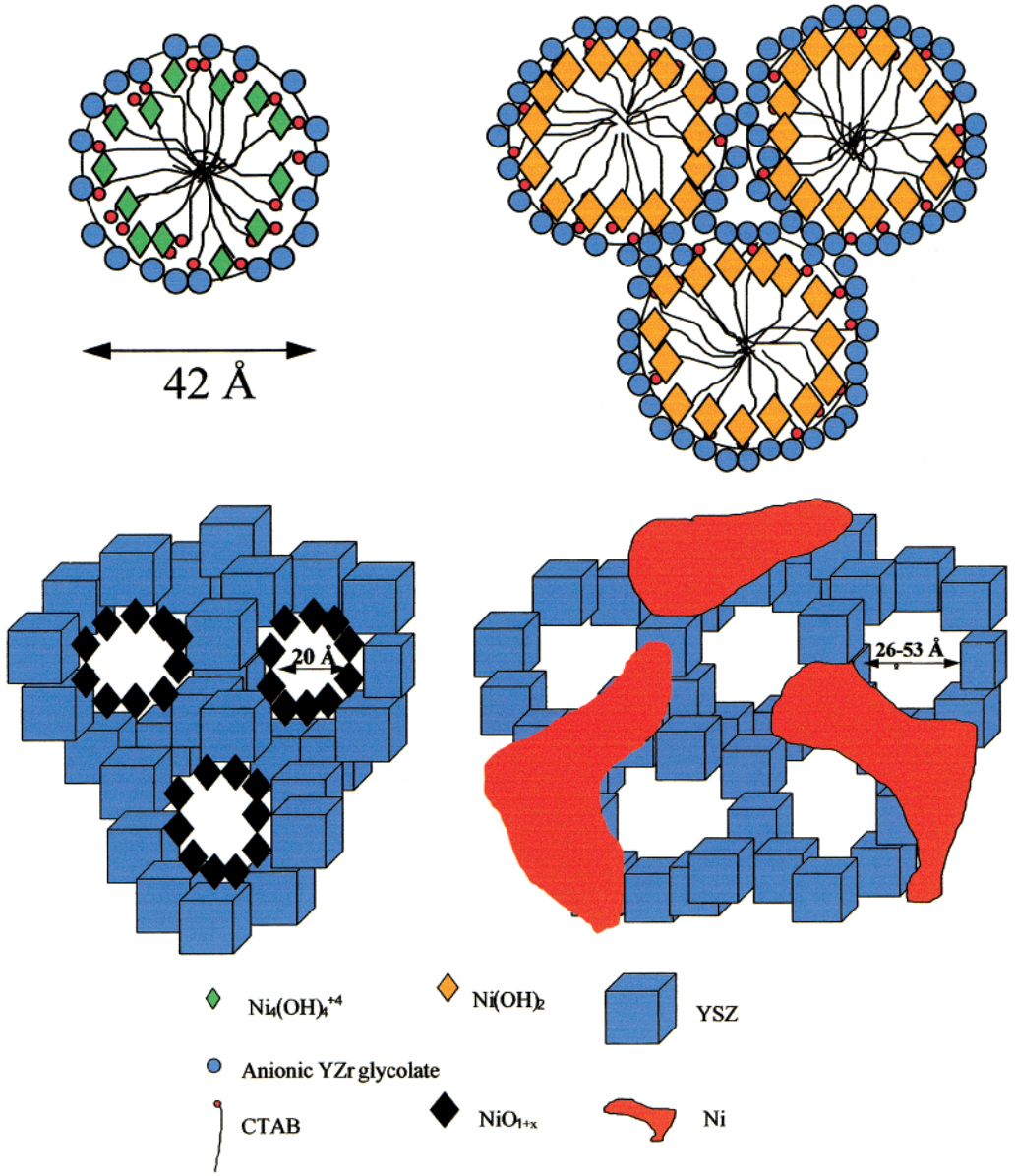

[a] Illustration of the surfactant-based Co-assembly of glycometalates of yttrium(III)−zirconium(IV) and $Ni_4(OH)_4^{4+}$ (top left), where in the synthesis the latter converts to X-ray amorphous $Ni(OH)_2$ nanoclusters (top right). Thermal treatment in air converts this material to meso-NiO_{1+x}–YZ with a worm-hole mesostructure and channel walls based on a contiguous assembly of nanocrystalline NiO_{1+x} and nanocrystalline YZ (bottom left). Thermal hydrogen reduction of meso-NiO_{1+x}–YZ creates the final product meso-Ni−YZ, which has a worm-hole mesostructure and channel walls based on a contiguous assembly of nanocrystalline Ni and nanocrystalline YZ (bottom right).

cationic surfactant. Upon adding the nickel salt, $Ni_4(OH)_4^{4+}$ is most likely incorporated in the liquid crystal templating phase at the interface between the anionic YZ glycolate and cationic surfactant headgroup, as illustrated at the top left of Scheme 1. The resulting green precipitate from the co-assembly process is shown at the top right of Scheme 1, where nickel in the mesostructure in the form of $Ni(OH)_2$ remains located near the surfactant headgroup−glycolate interface. Since PXRD analysis shows the as-synthesized product to be X-ray amorphous, it is likely that the $Ni(OH)_2$ exists as nanometer-sized clusters due to extensive X-ray line broadening. Upon thermal oxidation in air, a mesostructure is formed in which the walls are composed of nanocrystalline yttria−zirconia and the $Ni(OH)_2$ is converted to nanocrystalline NiO_{1+x} somehow integrated on the channel walls. The variability of the pore diameter and low-angle *d* spacing as previously discussed is a direct result of the amount of $Ni_4(OH)_4^{4+}$ incorporated in the aqueous phase. As more $Ni_4(OH)_4^{4+}$ is incorporated at the surfactant headgroup−glycolate interface, larger and/or higher populations of NiO_{1+x} nanocrystallites are formed on calcination. Larger pore diameters at higher NiO_{1+x} content may be ascribed to a type of scaffolding effect whereby the NiO_{1+x} nanocrystallites in the YZ walls maintain open pores as crystallization occurs. Thus, higher NiO_{1+x} loadings lead to larger pores, thicker walls, and a higher PXRD *d* spacing. When reduction occurs, Ni diffuses from within the pores of the mesostructure formed by the YZ walls to form larger aggregates, bottom left and right of Scheme 1. This process is accompanied by a decrease in unit cell volume in going from nanocrystalline NiO_{1+x} (11.1 cm^3/mol) to nanocrystalline Ni (6.6 cm^3/mol).[14] At

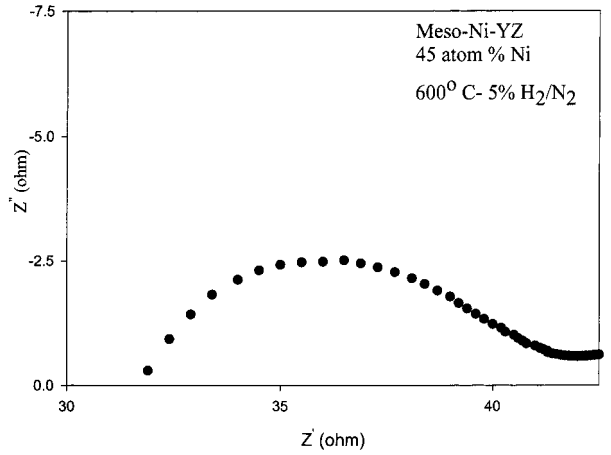

Figure 8. Complex impedance Argand plot for 45 Ni at. % loaded meso-Ni−YZ recorded at 600 °C in 5% H2/N2.

small Ni loading the NiO_{1+x} phase tends to be highly dispersed throughout the pore structure, leading to incomplete pore wall coverage where the NiO_{1+x} phase could exist as discrete, isolated nanocrystallites resulting in irregular scaffolding, smaller average pore sizes, and a wider pore size distribution, which become more evident upon NiO_{1+x} reduction. At higher loading, the pore wall coverage of NiO_{1+x} is more extensive and homogeneous in nature, where the NiO_{1+x} nanocrystallites may be in direct contact with each other forming a contiguous network within the YZ pores. Since the NiO_{1+x} coverage is more uniform at higher loading, then as nickel migrates within the pores during the reduction process, much larger pores with a narrow size distribution are left behind from the assembly of YZ nanocrystallites.

Preliminary electrochemical measurements have consisted mainly of ac impedance spectroscopy.[15] Samples containing 40 at. % Ni or less gave a response typical for a porous network of nanocrystalline YZ with isolated Ni nanocrystallites interspersed throughout the YZ channel walls. Such samples gave a single, slightly depressed complex impedance semicircle from 400 to 700 °C under a reducing atmosphere. The resistance, as determined from the diameter of the semicircle, decreased as the temperature increased, giving an activation energy similar to that of the bulk form of YSZ (100 kJ/mol). Upon increasing the loading to 45 Ni at. %, a metallic response was observed with increasing temperature. While loading values below 45 Ni at. % resulted in conductivity values in the range of 1×10^{-6} to 1×10^{-8} ohm^{-1} cm^{-1}, a loading of 45 Ni at. % resulted in a conductivity of 0.03 ohm^{-1} cm^{-1}. A representative complex impedance plot is shown in Figure 8. This dramatic increase in conductivity can be attributed to better connectivity between Ni nanocrystallites although the electronic percolation threshold has not yet been reached.[16] Some migration and agglomeration of Ni nanocrystallites as well as grain growth of YZ is observed in samples subjected to the measurement conditions described above. For example, PXRD analysis of the 45 Ni at. % sample shows the Ni nanocrystallite size to have increased from 151 to 252 Å, while nanocrystalline YZ is estimated to have grown from about 25−30 to 80 Å. Further electrochemical measurements such as studying the current/voltage characteristics are planned where meso-Ni−YZ will be used as the anode in a SOFC test cell.

Conclusion

Meso-Ni−YZ has been synthesized by surfactant-based co-assembly of glycometalates of yttrium(III)−zirconium(IV) and nickel(II) precursors followed by calcination to meso-NiO_{1+x}−YZ and finally hydrogen reduction to the desired product. The mesostructure of meso-Ni−YZ is an integration of nanocrystalline nickel and nanocrystalline yttria−zirconia channels in a wormhole arrangement. The material has a high surface area and a narrow pore size distribution combining an oxygen ion conductor and nickel electronic conductor at the nanometer scale. Metal loading of 0−40 Ni at. % gives an ac impedance response dominated by the oxygen ion−conductive YZ phase while higher loading shows a metallic response due to enhanced connectivity between Ni nanoclusters. It is envisioned that such a material may have potential utility as the fuel electrode in low-temperature solid oxide fuel cells.

Acknowledgment. We are deeply indebted to the Natural Sciences and Engineering Research Council of Canada (NSERC) for support of this work. Technical assistance with the synthesis of samples by Ms. Gabriella Metreux is greatly appreciated. We thank Michal Kruk at the Department of Chemistry, Kent State University, for helpful technical advice with analysis of gas adsorption data of materials close to the meso-/microregime.

CM001259J

(14) Mogensen, M.; Primdahl, S.; Jorgensen, M. J.; Bagger, C. *J. Electroceram.* **2000**, *5*, 141.

(15) MacDonald, J. R. *Impedance Spectroscopy*; John Wiley & Sons, Ltd.: New York, 1987.

(16) (a) Dees, D. W.; Claar, T. D.; Easler, T. E.; Fee, D. C.; Mrazek, F. C. *J. Electrochem. Soc.* **1987**, *134*, 2141. (b) Anselmi-Tamburini, U.; Chiodelli, G.; Arimondi, M.; Maglia, F.; Spinolo, G.; Munir, Z. A. *Solid State Ionics* **1998**, *110*, 35.